

Numerical Model-Based Optimization of Mining-reinjection Balanced Sustainable Exploitation Scheme for Geothermal Mine with Layered Karstic Reservoir

Li Yang^{1,2}, Dongdong Yue^{1,2}, Zhaolong Feng^{1,2}, Jian Song^{1,2}, Qiuxia Zhang^{1,2}, Donglin Liu^{1,2}, Xiaofeng Jia^{1,2}, Shengtao Li^{1,2,*}

¹Center for Hydrogeology and Environmental Geology Survey, China Geological Survey, Baoding 071051, China

²Tianjin Engineering Center of Geothermal Resources Exploration and Development, Tianjin 300300, China

yli_b@mail.cgs.gov.cn, lishengtao@mail.cgs.gov.cn *

Keywords: modeling, optimization, Mining-reinjection Balance, sustainability, thermal breakthrough

ABSTRACT

China is the Worldwide leader in geothermal energy direct use. Some cities in the North China Plain, such as Xiong'an and Tianjin, have achieved large-scale geothermal district heating by taking advantage of their excellent Mesoproterozoic karstic heat reservoirs and attracted global attention. With the rapid development of the utilization scale, more geothermal energy will be needed. Therefore, a sustainable exploitation scheme will be essential for a higher geothermal resource development degree. In recent years, the mining-reinjection balanced mode has been the compulsory management required to take the heat without water consumption. On this background, sustainable exploitation still faces many challenges, like a degree of geothermal fluid temperature drop, Heat breakthrough, and overlarge drawdown can all be constraint factors. A geothermal exploitation block with a certain degree of development in Rongcheng county is chosen for the sustainable scheme optimization study. Based on a numerical hydro-heat model with reliable parameter estimation derived from production and tests, temperature and pressure fields of the mining area with different (1) distances of production and reinjection wells, (2) single-well yields, and (3) reinjection temperatures are compared and discussed. The results can provide a scientific basis and accurate guidance for capacity expansion for the mining block in the near future.

1. INTRODUCTION

The Earth is a large heat reservoir, and the deeper the Earth goes inside, the hotter it gets. The energy transferred from the Earth's interior to the surface daily is equivalent to 2.5 times the daily energy consumed by all humans (Wang J Y et al., 2005). This heat stored in the Earth's interior is far more abundant than fossil fuels. As a kind of clean energy, geothermal energy has attracted more and more attention in the context of global climate change and environmental pollution.

It is estimated that in North China, there are 42.3 days on average every year suffering from smog from 1999 to 2013 (X. Li., 2016), with the mean PM_{2.5} concentration reaching 93 $\mu\text{g}/\text{m}^3$ (Ministry of Environment Protection of the People's Republic of China, 2015). It is critical to increase the use of clean energy and reduce the proportion of fossil fuels in total energy consumption. As one of the most vital renewable and clean energy, geothermal energy is expected to occupy 3% of total energy utilization in China by 2030, which will be mainly used for heat supply in winter (J. Hou, M. Cao, P. Liu. 2018). Most of the geothermal reservoirs in China belong to typical medium-low temperature geothermal resources.

At the 2010 World Geothermal Congress in Bali, delegates pointed out that one of the significant problems in geothermal development is the decrease of geothermal reservoir pressure caused by massive geothermal exploitation and the reduction of geothermal field production capacity. (Albert A. et al., 2010; Soheil P. et al. 2010; Einar G. et al., 2010) Reinjection is one of the essential means to ensure the stability of geothermal reservoir pressure and the sustainable development of the geothermal field. In the short term, geothermal water reinjection may add additional costs. But in a long time, it is necessary to maintain the reservoir's pressure, improve the recovery rate of heat energy, and extend the life of the geothermal field. Geysers geothermal fields in the United States experienced a sharp decline in productivity before reinjection and a 50% increase in productivity after reinjection measures were implemented. (Giovannoni A. et al., 1981; Cappetti G et al., 1982) In North China, the balance of production and reinjection has become a critical restraint means for the administrative department for geothermal exploitation.

The numerical model provides a very powerful help for predicting temperature and pressure changes in geothermal reservoirs. Several large geothermal fields around the world, examples include the Wairakei geothermal field in New Zealand (Zarrouk S. J. et al., 2006) and the Larderello geothermal field in Italy (Romagnoli P. et al., 2010) and others used numerical models to simulate and predict the changes of pressure, production, and enthalpy of geothermal reservoirs. With the further development and utilization of the geothermal field, the model is updated step by step to make the simulation result more accurate. The numerical model has become a relatively mature technology that can support the rational layout of geothermal Wells and the sustainable development and utilization of geothermal resources.

TOUGH2 is a program designed to simulate the multi-dimensional migration of multiphase and multicomponent fluids and heat flows in porous and fractured media. It simulates geothermal reservoirs, nuclear waste disposal, environmental assessment and remediation, fluid flow, and solute migration in variable saturated media and aquifers.

In this paper, a geothermal mining block in Rongcheng Geothermal Field, Xiongan New Area, is taken as the object. The numerical model is established using Tough2, and the parameters with high accuracy are obtained in the production stage. The response of the reservoir under the conditions of different mining strategies is simulated, and the optimal production parameters are finally obtained, which provides a scientific basis for the formulation of the geothermal resource exploitation scheme.

2. MATERIAL AND METHODOLOGY

2.1 Study area

Rongcheng County belongs to the Xiong'an New Area, located in the central Hebei plain, the hinterland of the Beijing-Tianjin-Baoding triangle. The geographical coordinates are 115°45' 26" to 116°04' 02" E and 38°57' 04" to 39°08' 32" N. It is 26.85km long from east to west and 21.38km wide from north to south, with a total area of 314 km². Roads and railways are well developed. (Figure 1)

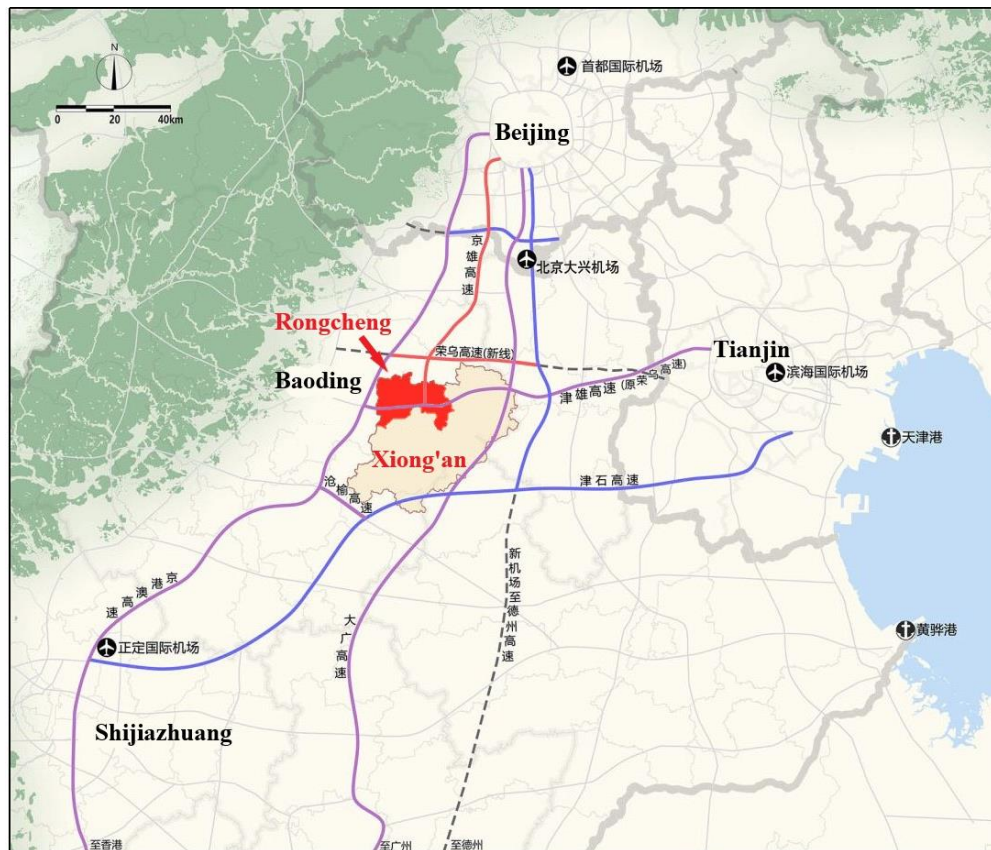


Figure 1: Location map of Rongcheng County.

Rongcheng County is in the eastern foot of Taihang Mountain, the middle of Jizhong plain, on the alluvial fan of the Daqing River system, belonging to the transition zone from Taihang piedmont plain to the alluvial plain. The county is higher in the northwest, slightly lower in the southeast, and 7-19m above sea level. Rongcheng County is in the warm temperate continental monsoon climate zone, with four distinct seasons. The average annual temperature is 11.9°C, and the average annual precipitation is 517.8mm.

2.2 Geological setting

Rongcheng geothermal field, centered on the Rongcheng uplift, is a secondary forward structure in the Jizhong Depression (Figure 2). It is located northeast of the Jizhong Tai Depression, controlled by the Xushui fault and Rongcheng fault, and forms Rongcheng low uplift area. The north is the Langgu Depression, the south is the Baoding depression and the Gaoyang low uplift, the west is the Xushui depression, and the east is the Niutuozen uplift. The regional geothermal background of the Rongcheng geothermal field is the hot basin area in eastern North China, which has a high heat flow background. The axis of the Rongcheng uplift is trending toward the northeast, consistent with the direction of the main tectonic line fracture in the area, and the buried depth of the bedrock in the geothermal field is less than 1000m.

The surface outcropping layer of the Rongcheng geothermal field is Quaternary alluvial-diluvial loose strata. The strata below Quaternary include Neogene, Paleogene, Ordovician, Cambrian, Middle and Upper Proterozoic, Archaean, and so on. (Figure 3)

The geothermal reservoirs in Rongcheng geothermal field include the pore sandstone reservoir of the Neogene Minghuazhen Formation and bedrock reservoirs of Cambrian, Jixian and Changcheng Systems. The carbonate rocks of the Jixian Formation are the main geothermal reservoirs, including Wumishan and Gaozhuang Formations, which are deep circulation karst fractured geothermal reservoirs formed under the joint action of heat conduction and heat convection. The lithology of the strata is mainly macrubble band dolomite and dolomite. The strata in this section have experienced weathering, denudation, and leaching in a long geological period, providing a good groundwater storage space.

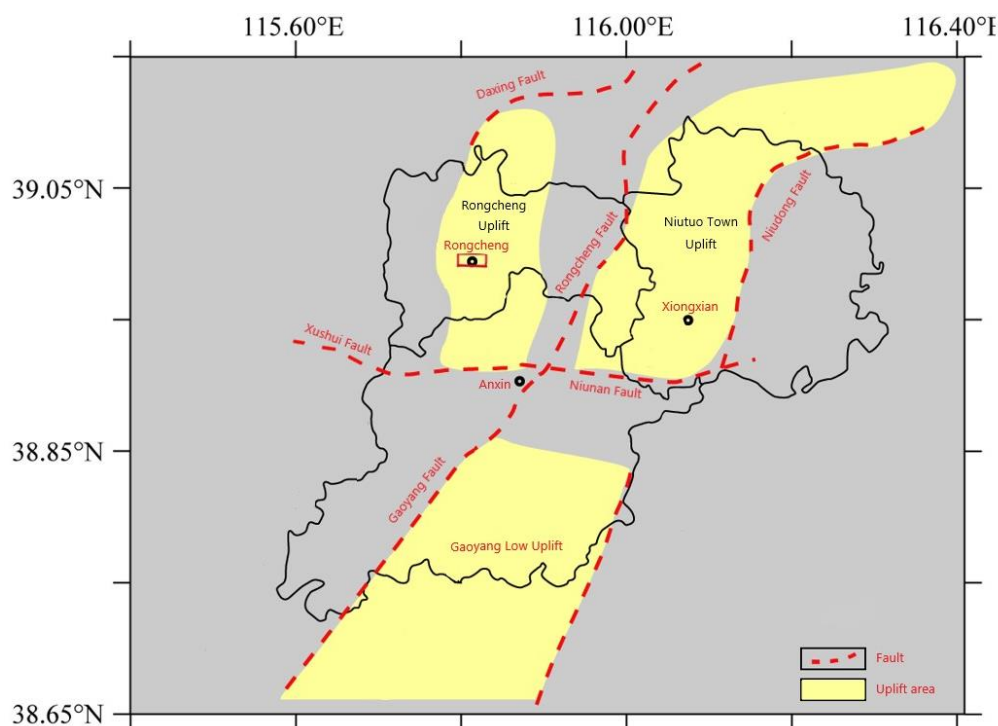


Figure 2: Tectonic geological map of Rongcheng County.

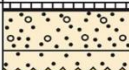
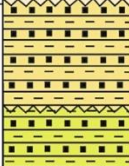
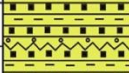
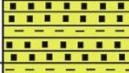
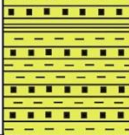
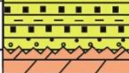
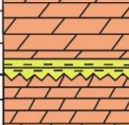
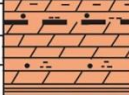
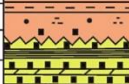

| Age (Ma) | Strata system | | | Thickness (m) | Lithology | Description | |
|-------------------------|------------------------------|------------|--|---|--|--|--|
| 2.58 | Kz | Quaternary | | Pingyuan Formation (<i>Qp</i>) | 430~450 |  | Plow soil, gravel, silt, medium sand |
| | | N | N2 | Minghuazhen Formation (<i>Nm</i>) | 600~820 |  | Sandstone mudstone interbed |
| N1 | | | Guantao F. (<i>Ng</i>) | 0~200 |  | Sandstone, mudstone, and conglomerate | |
| E | | E3 | Dongying Formation (<i>Ed</i>) | 0~300 |  | Sandstone, mudstone | |
| | | E2 | Shahejie Formation (<i>Es</i>) | 0~600 |  | Mudstone, oil shale, sandstone | |
| | | E1 | Kongdian F. (<i>Ek</i>) | 0~260 |  | Sandstone, mudstone, and conglomerate | |
| | | Pz | Є | Chaomid F. (<i>Єc</i>) | 0~200 |  | Limestone dolomite, mudstone, and conglomerate |
| Gushan F. (<i>Єg</i>) | | | | 0~400 | | | |
| Mantou F. (<i>Єm</i>) | | | | 0~500 | | | |
| 1400 | | Pt | Jx | Tieling F. (<i>Jxt</i>) | 0~600 |  | Dolomite; Quartz sandstone; Marl rock |
| | Hongshuiz. F. (<i>Jxh</i>) | | | 0~400 | | | |
| | Wumishan F. (<i>Jxw</i>) | | | 300~1200 | | | |
| | Yangzh. F. (<i>Jxy</i>) | | | 0~150 | | | |
| | Gaoyuzh. F. (<i>Jxg</i>) | | | 0~1000 | | | |
| | Ch | | Dahongyu F. (<i>Chd</i>) | 0~300 |  | feldspar quartz sandstone; dolomite with shale; sandstone. | |
| | | | Tuanshanzi F. (<i>Chr</i>) | 0~200 | | | |
| | | | Chuanl. F. (<i>Chd</i>) | 0~200 | | | |
| 1800 | Ar | | | |  | Gneiss | |

Figure 3: Typical stratigraphic comprehensive histogram of Rongcheng geothermal field.

2.3 Conceptual model

Due to the failure of the craton, heat from deep transmits to the surface in the form of heat conduction, forming thermal refraction in the carbonate rocks with high thermal conductivity and forming thermal reflection in the sedimentary cover with low thermal conductivity in the shallow surface. At the same time, it overlaps the circulation of regional groundwater and water-rock heat exchange, forming a stable and high-quality geothermal reservoir under the multiple heat accumulation mode. (Figure 4)

2.3.1 Heat resource

From a regional perspective, the heat source comes from three aspects. First, the subduction of the western Pacific plate and the upwelling of the deep mantle material in North China promote the stable craton destruction, which then leads to the thinning of the crust and the phenomenon of Moho surface uplift and thinning, forming a regional stable high heat flow background. Second, the heat flow accumulation of carbonate rocks with high thermal conductivity is mainly due to heat flow into the upper crust. Under the restriction of the tectonic pattern of bedrock uplift and depression, heat flow is redistributed, and there is a tendency to tilt from the depression to the bulge at the junction of the structure. As a result, heat flux increases at the bulge and decreases at the depression. Third, the heat increase of groundwater from the piedmont to the deep geothermal reservoir recharge process.

2.3.2 Geothermal reservoir

The thermal reservoir of the Wumishan Formation in the Jixian system is mainly evaluated in this paper. The stratigraphic lithology is predominantly gray and grayish-white macelstone-bearing strip dolomite and dolomite. The strata in this section have experienced denudation, weathering, and leaching in a long geological period. The dissolved rock gaps and fractures are relatively developed, providing good storage space for groundwater. Due to the influence of regional secondary structure and weathering denudation, the Wumishan Formation is partially missing in the center of the bulge structure, and the thickness of the Wumishan Formation increases significantly from the center of the bulge to the two wings, with the maximum thickness of about 1000m.

2.3.3 Cap rock

The Quaternary system is widely distributed in the area, with a thickness of about 400m, and its lithology is mainly composed of subsandy soil, sub clay, clay, and sand layers. It has the characteristics of loose deposition and poor thermal conductivity. When heat flow from deep underground passes through the layer to the surface, the heat can be saved in the geothermal reservoir because of the apparent reduction of thermal conductivity rate. This area has good conditions for geothermal reservoir cover. Neogene strata not only has the function of the geothermal reservoir but also is a good cap rock for overlying reservoirs.

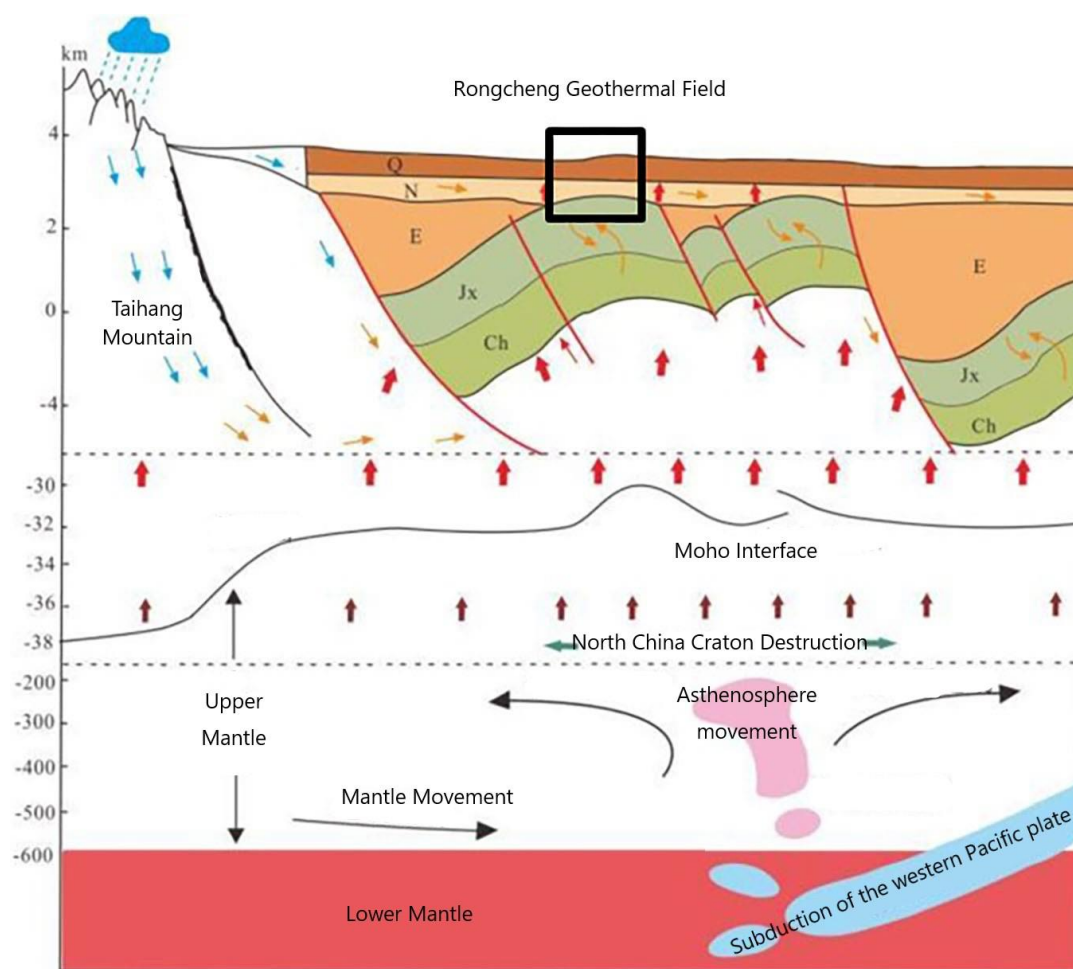


Figure 4: Geothermal conceptual model of Rongcheng geothermal field.

2.4 Methodology

This study employed the coupled Thermal-Hydrologic (TH) model for simulating processes in geothermal reservoirs within fractured porous media.

Energy and mass equation solved by TOUGH2 can be expressed as below:

$$\frac{d}{dt} \int_{V_n} M^\kappa dV_n = \int_{\Gamma_n} F^\kappa \cdot n d\Gamma_n + \int_{V_n} q^\kappa dV_n \quad (1)$$

where, V_n is surrounded by closed border, M - mass/energy per unit volume; F is mass or heat flow, q is the source or sink, n is A normal vector of a surface element, the direction is going to be inside of V_n .

The general form of mass accumulation is as follows:

$$M^\kappa = \Phi \sum_{\beta} S_{\beta} \rho_{\beta} X_{\beta}^{\kappa} \quad (2)$$

Where, Φ is porosity, S_{β} is the saturation of β , ρ_{β} is the density of β , X_{β}^{κ} is the κ 's mass fraction of β .

The general form of heat accumulation in a multiphase system is:

$$M^{NK+1} = (1 - \Phi) \rho_R C_R T + \Phi \sum_{\beta} S_{\beta} \rho_{\beta} u_{\beta} \quad (3)$$

Where, ρ_R is the density of the rock, C_R is the specific heat content, T is the temperature, u_{β} is the inner energy of β .

The convective mass flow is the sum of the phases and is represented by the following equation:

$$F^{\kappa}|_{adv} = \sum_{\beta} X_{\beta}^{\kappa} F_{\beta} \quad (4)$$

Moreover, various phase flows can be expressed by Darcy's law of multiphase states:

$$F_{\beta} = \rho_{\beta} u_{\beta} = -k \frac{k_{r\beta} \rho_{\beta}}{\mu_{\beta}} (\nabla P_{\beta} - \rho_{\beta} g) \quad (5)$$

Where, u_{β} is the Darcy velocity of phase β , k is the absolute permeability rate, $k_{r\beta}$ is the relative permeability of phase β , μ_{β} is the viscosity of phase β .

Heat flow includes conduction and convection components:

$$F^{NK+1} = -\lambda \nabla T + \sum_{\beta} h_{\beta} F_{\beta} \quad (6)$$

Where, λ is the heat conductivity, h_{β} is the enthalpy of phase β .

3. MODELING

3.1 Model domain and boundary

The geothermal mining block in this study is in the Rongcheng geothermal field, a rectangular block with an area of about 15 km², about 5km long from east to west, and 3km wide from north to south. This block is in Rongcheng urban area, surrounded by geothermal mining blocks or proposed blocks. The thermal water storage force gradient of the Wumishan Formation in this area is relatively gentle. Considering that there are no large faults in and around the block and other factors that may influence the flow field and thermal field, the scope of the mining block is taken as the boundary of the model without extension. To reduce the uncertain influence of the bottom boundary on the model, the depth of the model is extended to 10km. Therefore, the boundary conditions of the model are set as follows:

- 1) The top boundary is the constant temperature zone, then set as the constant temperature boundary, and the top and bottom hydraulic boundaries are the no-flow boundary.
- 2) The bottom boundary is preset to a constant temperature boundary of 245 °C, which will be adjusted according to the fitting results of the thermal storage temperature field.
- 3) The side boundary is no flow boundary.

3.2 Discretization

According to the distribution of buried depth of roof and floor in different strata, the geological model of the block was established, including the Quaternary, Neogene Minghuazhen Formation and the Wumishan Formation of the Jixian system and the shallower strata. The depth of the model ranges from 0 to 10000m, in which the grids with a thickness of 200m were set for 0-4000m depth, and the grids with 1000m thickness were set for subdivision in the depth range from 4000 to 10000m. The boundary of the geothermal mining block was taken as the model boundary. The surrounding area of the well was finely discretized, and the mesh size was about

25m×25m. Tyson polygon was used to divide the area, and the total mesh number of the geothermal mining blocks was 85,372 (Figure 5).

3.3 Initial condition

3.3.1 Thermal field

Taking the constant temperature zone temperature of 14.5°C as the benchmark, the regional 3D geothermal field is constructed according to the geothermal gradient distribution of the cap layer and thermal reservoir obtained by analysis.

The three-dimensional geothermal temperature distribution in the geothermal exploitation area is shown in Figure 6.

3.3.2 Flow field

The water level pressure data of the Wumishan Formation heat reservoir in the Rongcheng area were obtained, and the grid pressure value was calculated as the initial pressure condition of the model.

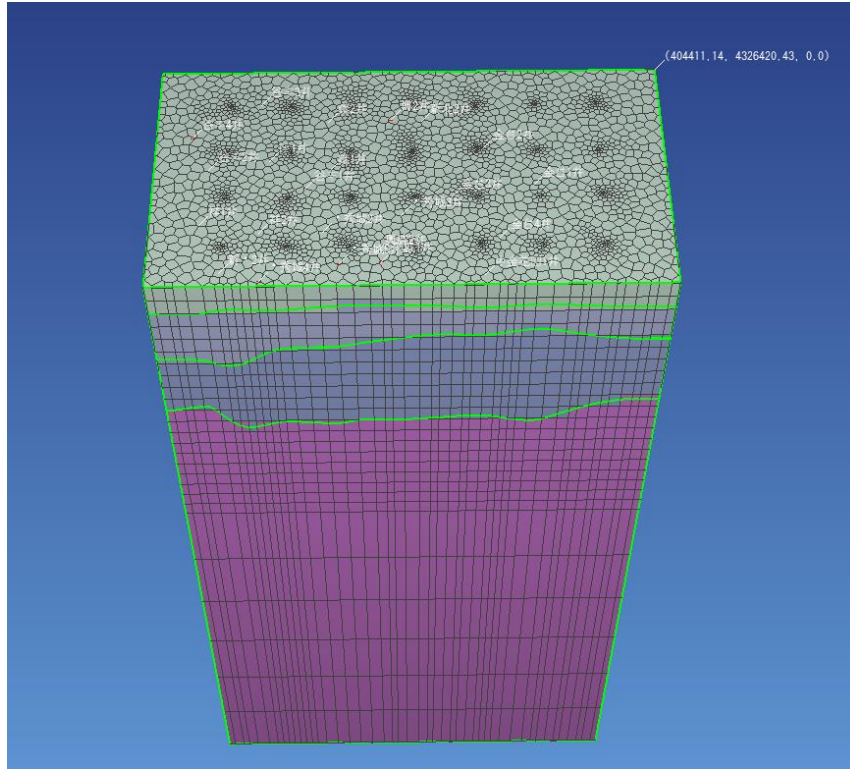


Figure 5: Model discretization.

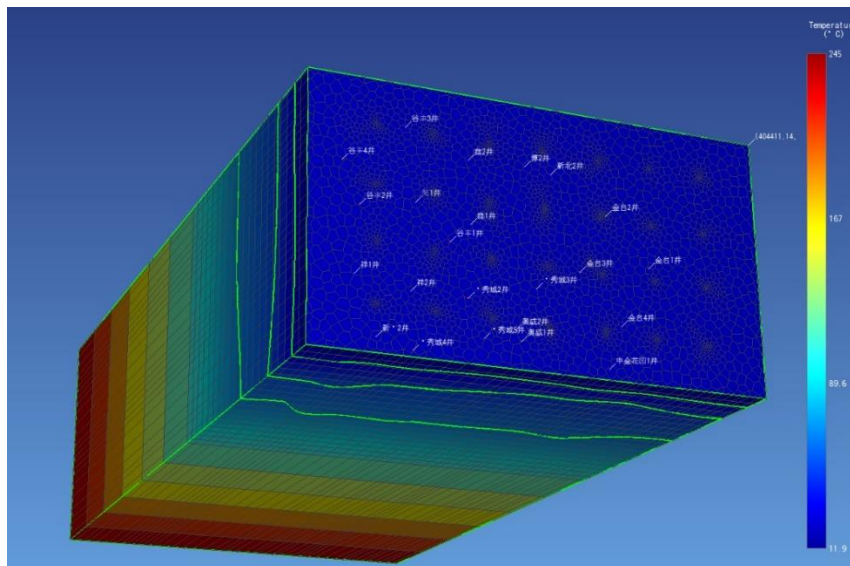


Figure 6: 3D geothermal field distribution map of mining block.

3.4 Calibration

3.4.1 Natural state

After several parameter adjustments, the geothermal field of the model is consistent with the current understanding of the geothermal field. It can truthfully reflect the temperature distribution in the exploration block, as shown in Figure 7.

3.4.2 Exploitation history match

Dynamic water level monitoring data of urban geothermal mining blocks in Rongcheng County were obtained through data collection, and model fitting was shown in Figure 8. The model results can fit with the historical monitoring data for many years, and the model results are reliable.

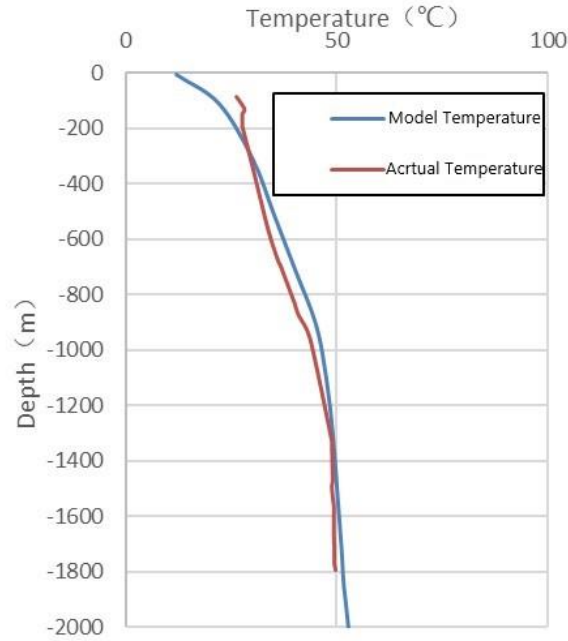


Figure 7: Temperature curve fitting of the model and actual data.

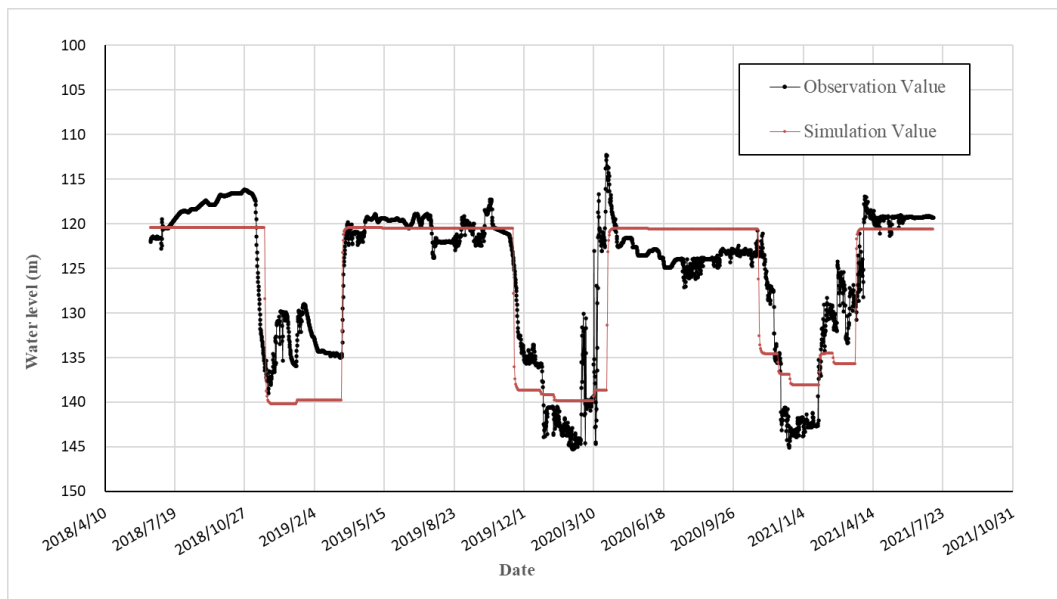


Figure 8: Mining history water level fitting map.

4. RESULTS AND DISCUSSION

The geothermal reservoir responses under different production schemes were analyzed, including centralized/decentralized production and reinjection, recharge temperatures, well spacing, and single-well production and reinjection volume. Taking November 15, 2019, as the starting time point of evaluation, the annual mining period was 120 days, and the total calculation time of the model was 100 years. Considering the constraint condition that a grid cannot cross a single time step, the adaptive time step was adopted for calculating time discretizing, the adjustment coefficient was set as 2, and the maximum time step was set as 30 days.

4.1 Centralized/distributed production and reinjection schemes

4.1.1 Distributed scheme

The layout of mining and irrigation Wells in the area adopts a 5-point type. To avoid thermal breakthroughs, the spacing of the production and reinjection wells was set to 600 meters. There were 14 production and reinjection wells in the block, a total of 28 geothermal wells, as shown in Figure 9. The production rate of a single well was $110 \text{ m}^3/\text{h}$ with 100% recharge and a recharge temperature of 25°C .

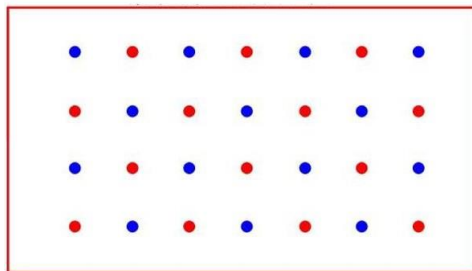


Figure 9: Diagram of distributed well layout scheme (blue point for production well and red point for reinjection well).

Figure 10 and Figure 11 show the changes in the bottomhole pressure of the production and reinjection wells, respectively. In contrast, Figure 12 and Figure 13 show the changes in the bottomhole temperature of the production and reinjection wells. During the heating period, the pressure at the bottom of the production well decreases and rises during the heating period. The bottomhole pressure of the recharge well increases during the production period and falls during the non-heating period. From the perspective of 100 years of the mining process, according to the results of the reinjection test, a mining rate of $110 \text{ m}^3/\text{h}$ can maintain the pressure balance of the reservoir and will not cause related geological disasters.

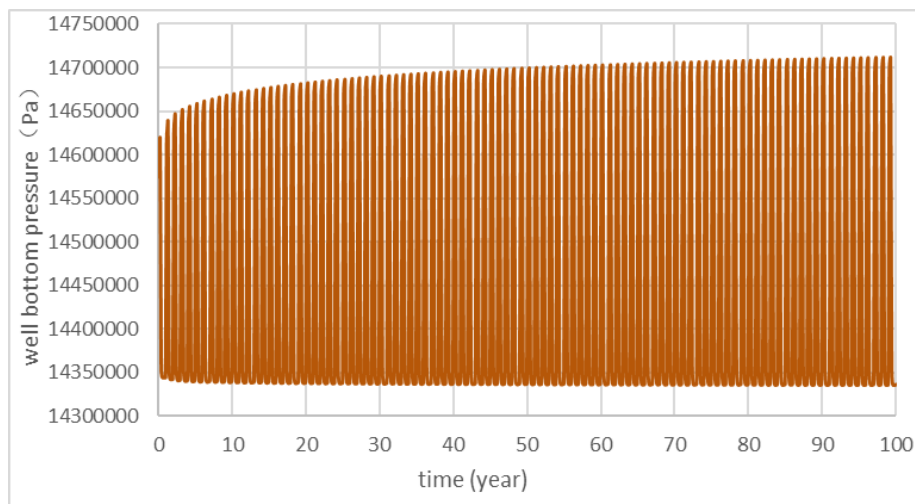


Figure 10: Bottom pressure variation diagram of typical reinjection well.

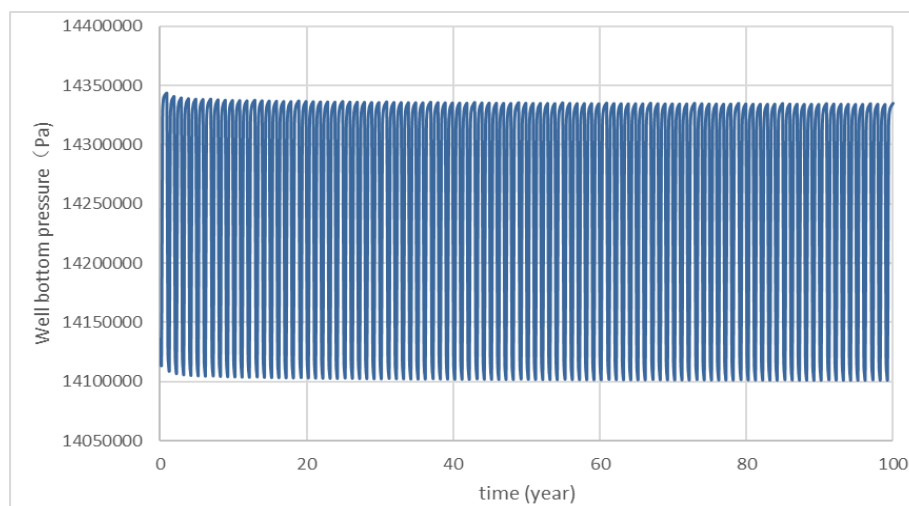


Figure 11: Bottom pressure variation diagram of typical production well

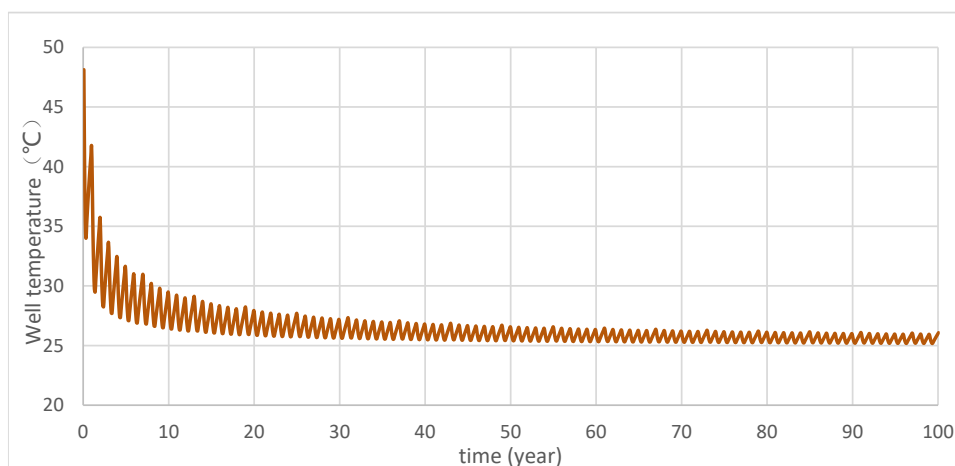


Figure 12: Bottom temperature variation diagram of typical reinjection well

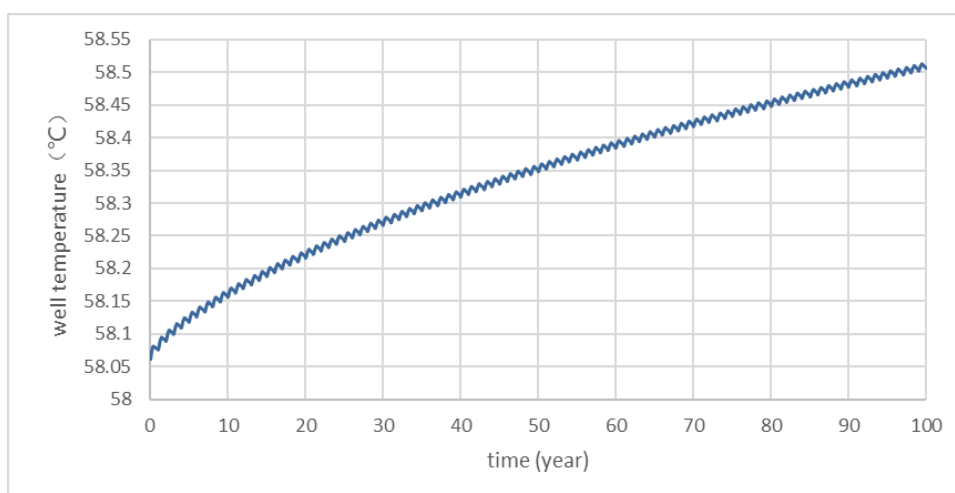


Figure 13: Bottom temperature variation diagram of typical production well

Reinjection caused the continuous temperature decrease around the reinjection well, and figure 14 shows the change in the geothermal field after 100 years of continuous mining. The maximum reduction reaches 30°C when the recharge water temperature is 25°C. Although there is a temperature drop around the recharge well, its influence range is only between 300 m and 350m, and no temperature drop occurs in the mining well. No thermal breakthrough occurs between the recharge well and the mining well. Therefore, the productivity of each mining well is stable.

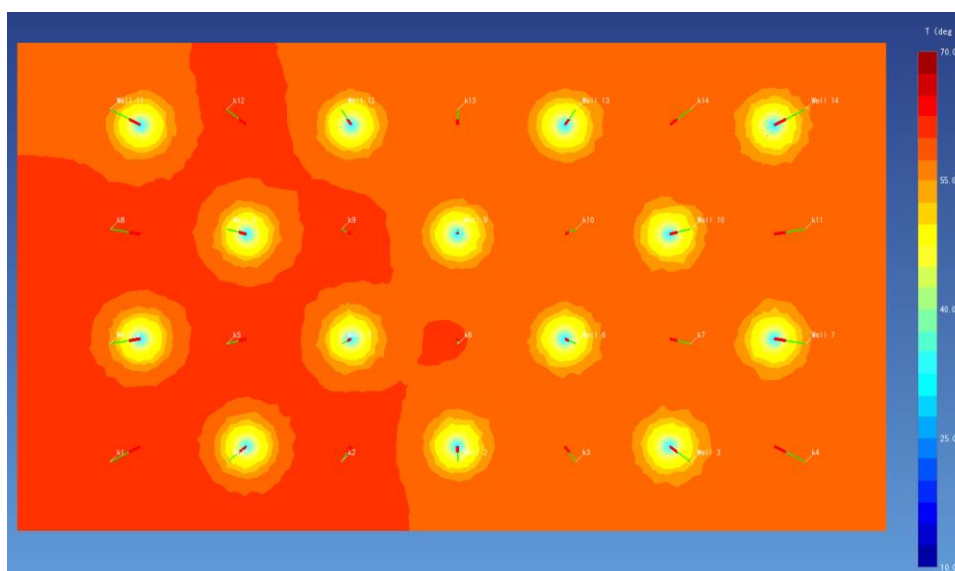


Figure 14: Distribution map of the geothermal field after 100 years of mining

4.1.2 Centralized scheme

The distribution of production and reinjection wells adopts the centralized distribution scheme, and the well spacing was set as 600m. 14 mining wells were arranged in the west, and 14 reinjection wells were placed in the east, as shown in Figure 15. The single well production rate is 110m³/h, 100% reinjection with a temperature of 25°C.

Figure 16 and Figure 17 show the changes in the bottomhole pressure of the production and reinjection wells, respectively, while Figure 18 and Figure 19 show the changes in the bottomhole temperature of the wells. From the perspective of 100 years of extraction and irrigation process, 110 m³ per hour of extraction and irrigation can maintain the reservoir's pressure balance.

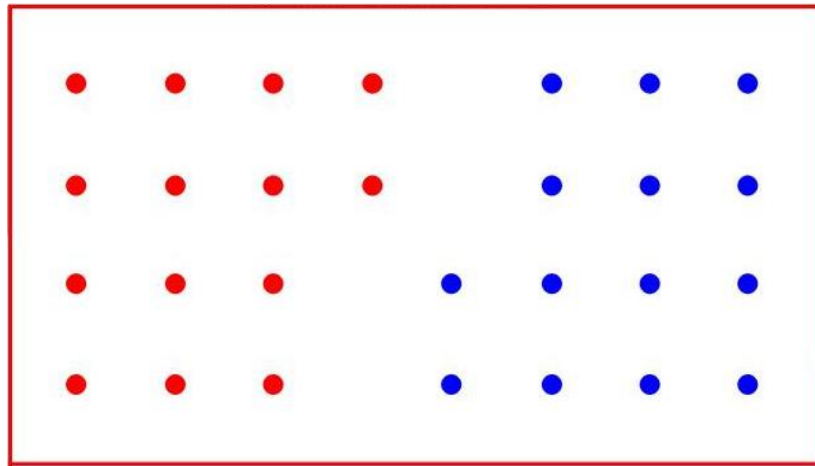


Figure 15: Diagram of centralized well layout scheme (blue point for production well and red point for reinjection well)

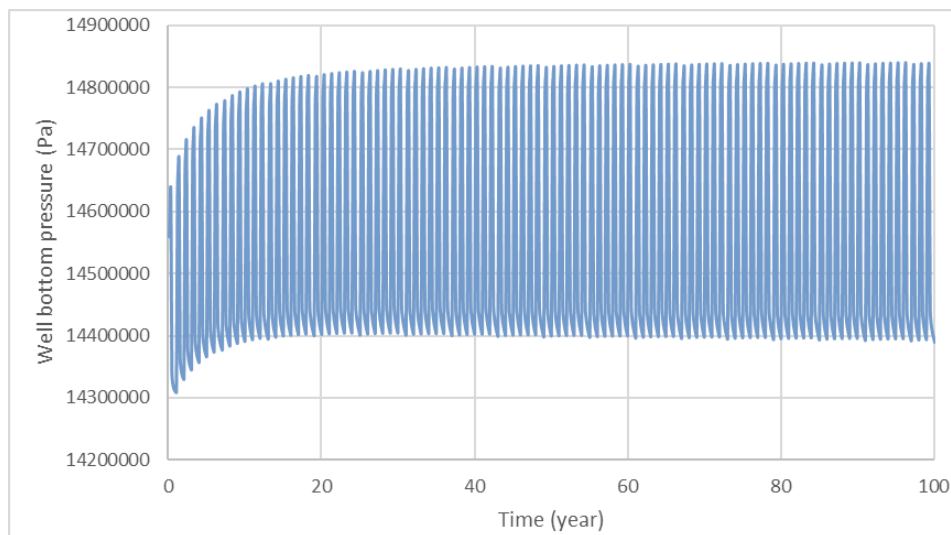


Figure 16: Bottom pressure variation diagram of typical reinjection well

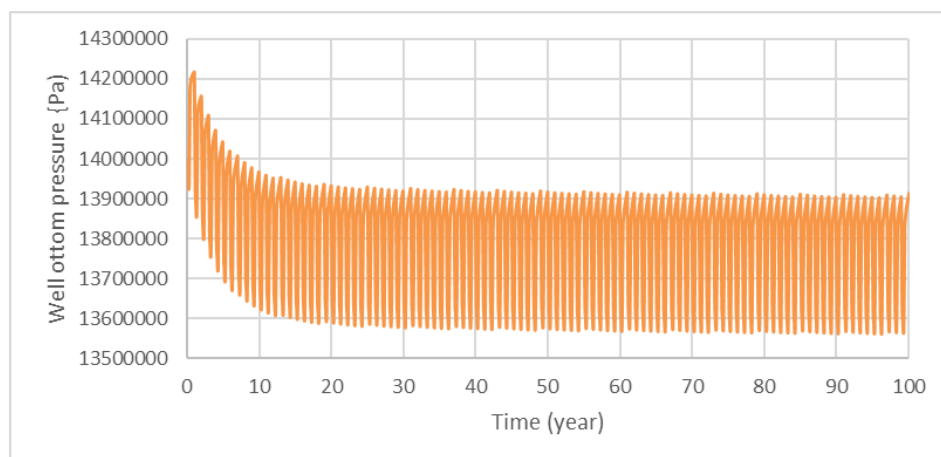


Figure 17: Bottom pressure variation diagram of typical production well

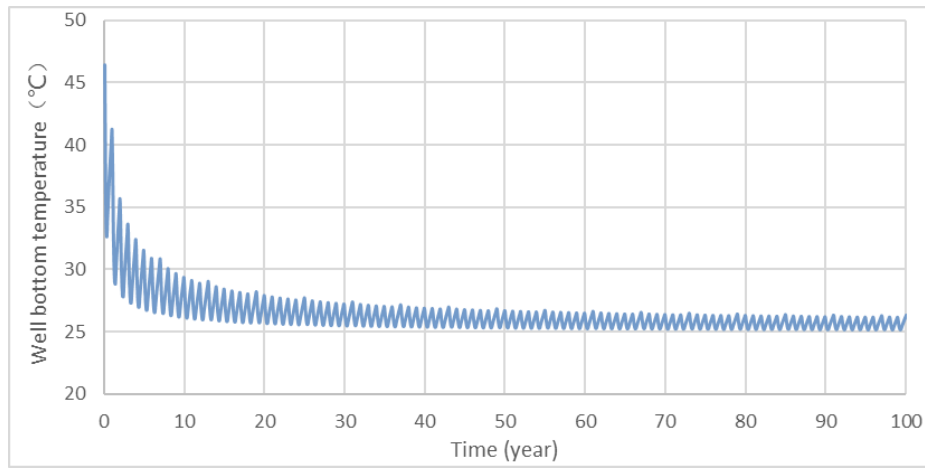


Figure 18: Bottom temperature variation diagram of typical reinjection well

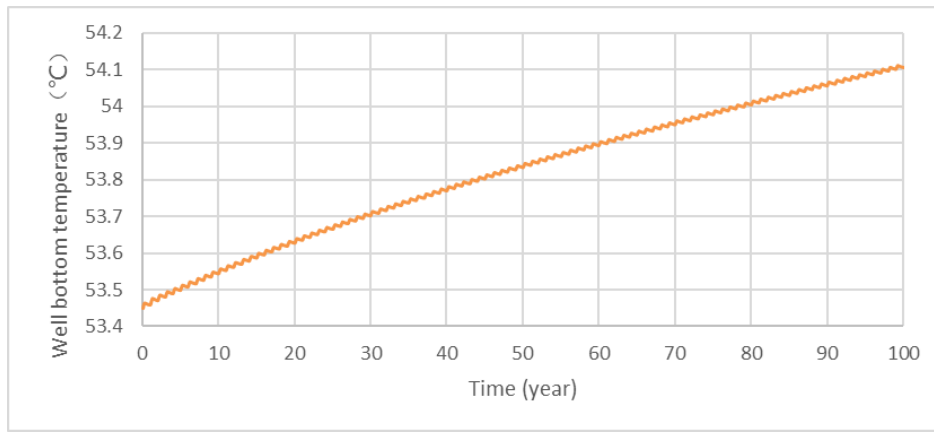


Figure 19: Bottom temperature variation diagram of typical production well

Figure 20 shows how the geothermal field changes after a 100-year mining period. It can be seen that the temperature of the production wells did not drop, and the average temperature was slightly higher than that under the distributed scheme. No thermal breakthrough occurred, and the productivity of each mining well was stable.

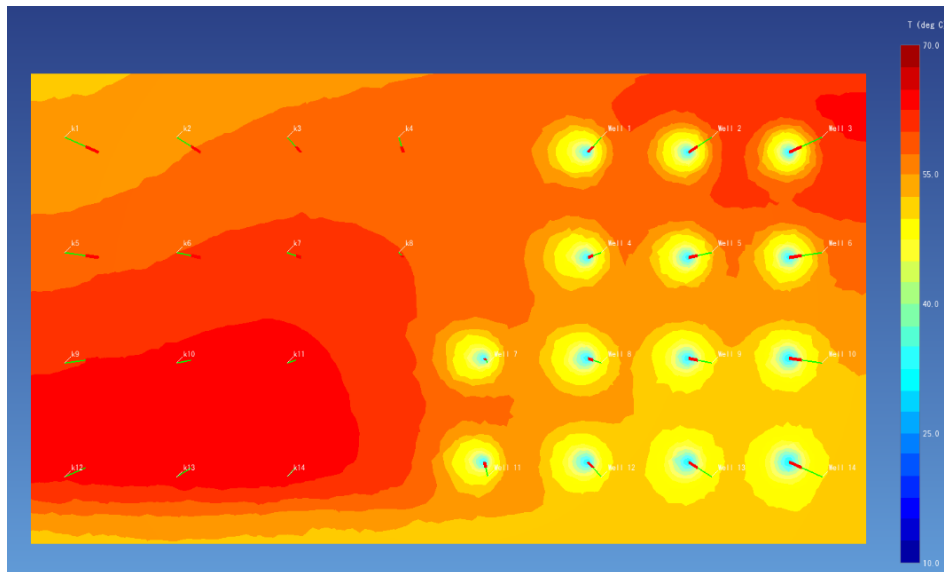
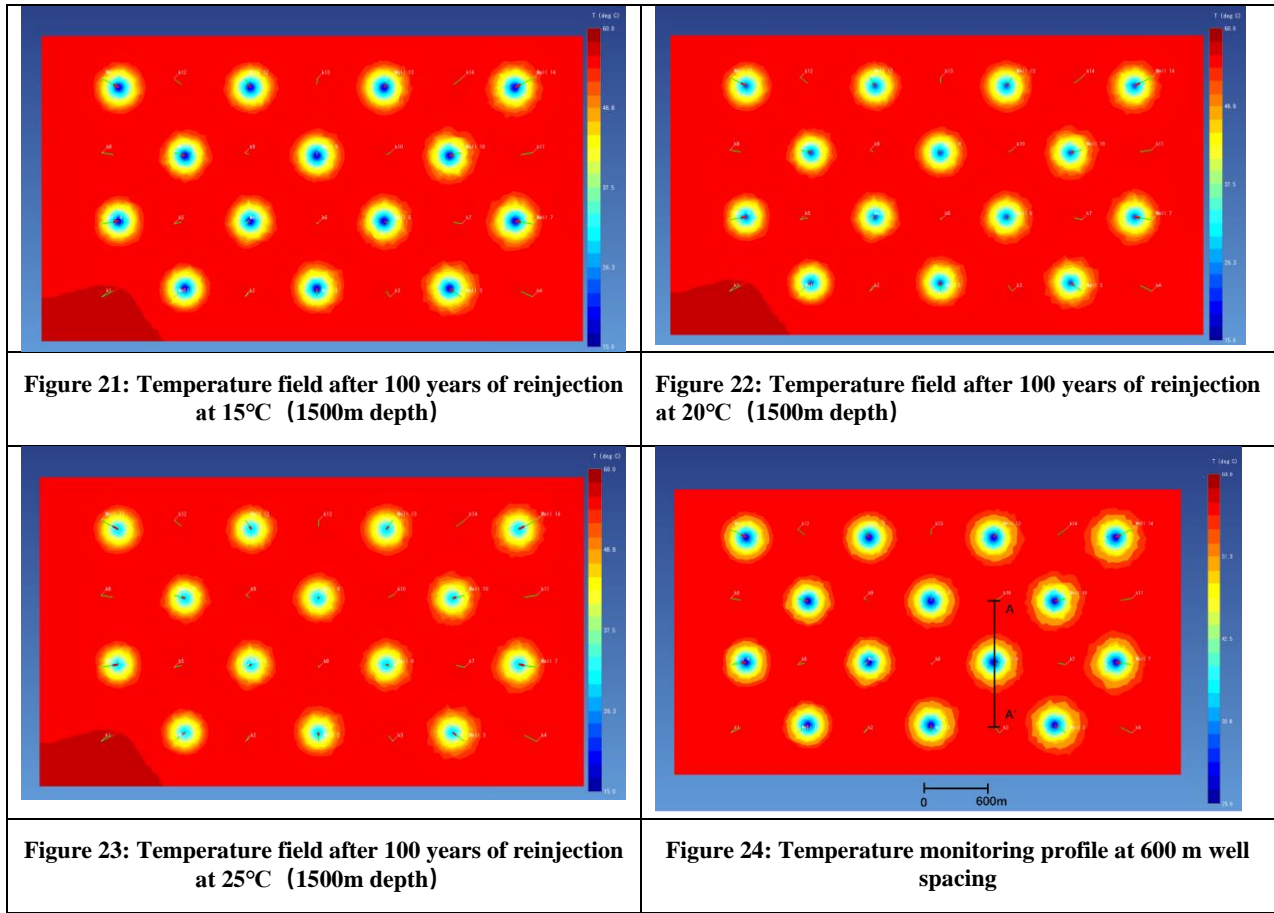


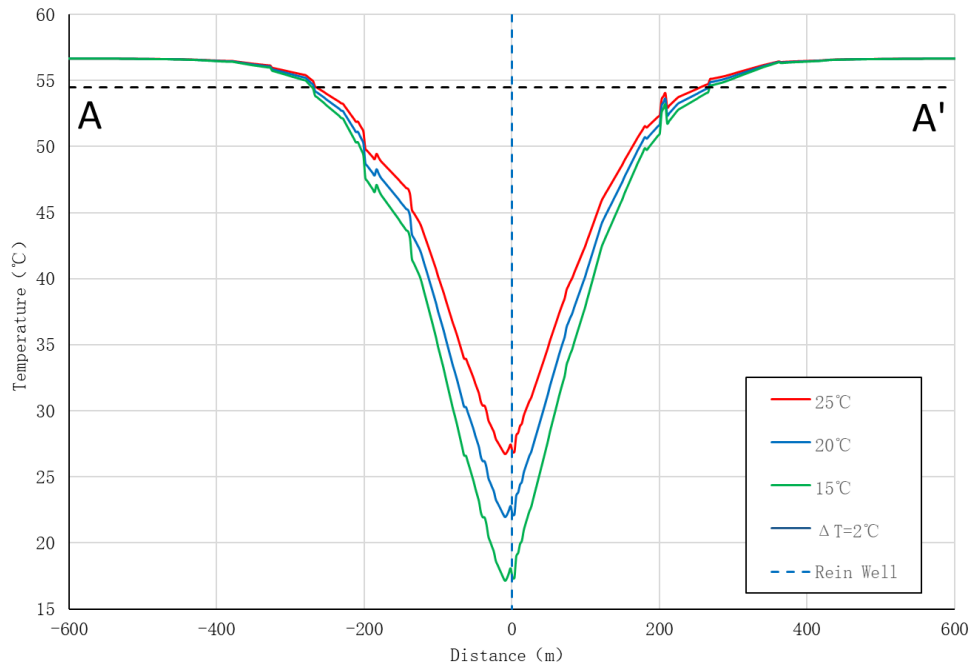
Figure 20: Distribution map of the geothermal field after 100 years of mining

4.2 Different reinjection temperature

The temperature field changes after 100 years under the conditions of 15°C, 20°C, and 25°C reinjection temperature were compared under 600m well spacing, as shown in Figure 21, Figure 22, and Figure 23.



As shown in the figure below, the distance of thermal breakthrough ($\Delta t > 2^\circ\text{C}$) under 600 m well spacing is about 500 m. Under the conditions of 15°C, 20°C, and 25°C, the temperature drop ranges were about 280 meters away from the reinjection well, and the temperature drop range of low-temperature reinjection was only about 10 meters compared with that of high-temperature recharge (Figure 25). The lower recharge temperature does not have a significant impact on the temperature drop range.



4.3 Different well spacing

According to the simulation results of 600m well spacing, the maximum influence range of the reinjection well was about 500 m, so 500 m well spacing was then used for the simulation. A total of 20 production wells and 20 reinjection wells were laid, and the well layout plan is shown in Figure 26.

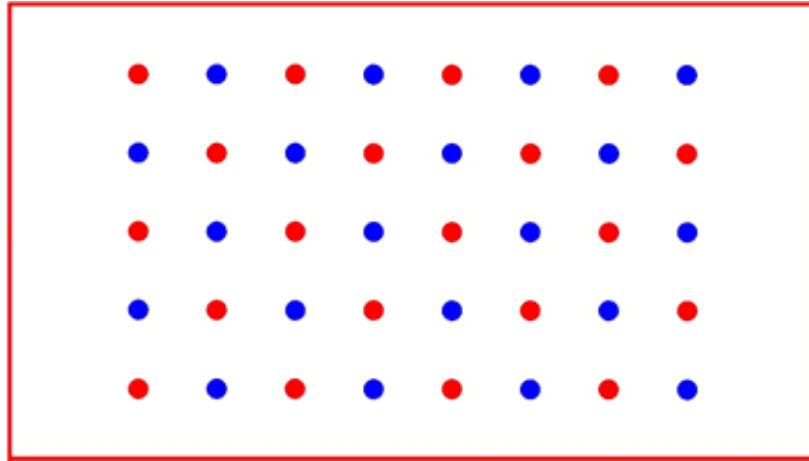


Figure 26: Diagram of well layout with the well spacing of 500m (blue point for production well and red point for reinjection well)

The comparison of temperature changes around the same reinjection well after 100 years with 500 m and 600 m well spacing is shown in Figure 27. Under 500 m well spacing, the temperature drop range was more significant than 600 m well spacing, and the temperature drop ($\Delta T > 2^\circ\text{C}$) range is between 280 m and 320 m. Due to the reduction of well spacing, the hydraulic field superposition between the production wells and the reinjection wells was more pronounced, resulting in the expansion of the influence range.

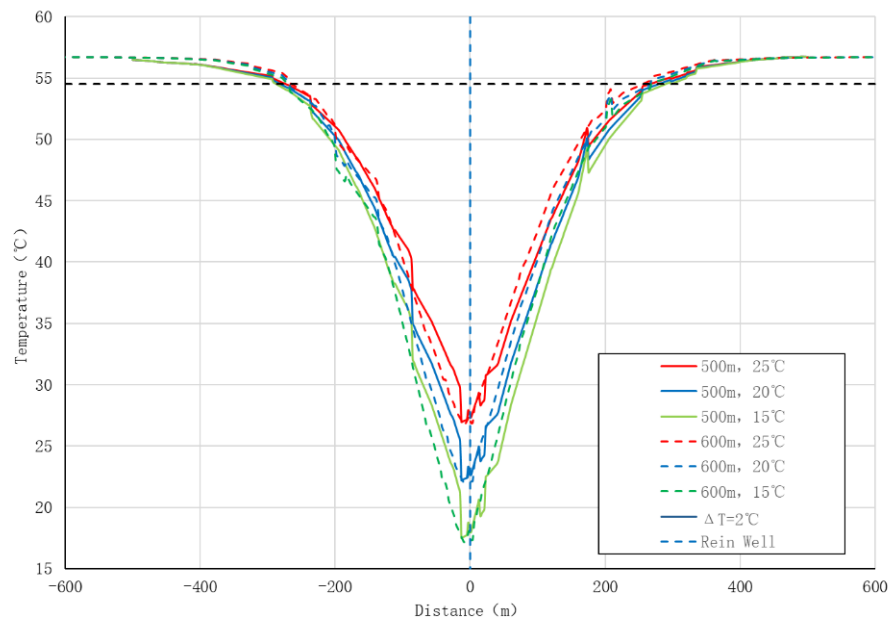


Figure 27: Comparison of temperature changes around the reinjection well after 100 years with 500 m 600 m well spacing

In terms of the production well temperature, under the same production rate ($110\text{m}^3/\text{h}$), the temperature did not decrease when the well spacing was 600 meters during the simulation period of 100 years, shown in Figure 28. However, when the well spacing was reduced to 500 meters, the production temperature declined after 50 years. It decreased by $0.1\sim 0.15^\circ\text{C}$ in 100 years, which did not exceed the present value of 2°C , which means no significant thermal breakthrough occurred. Based on the above simulation results, it is recommended that the well spacing should not be less than 500 meters.

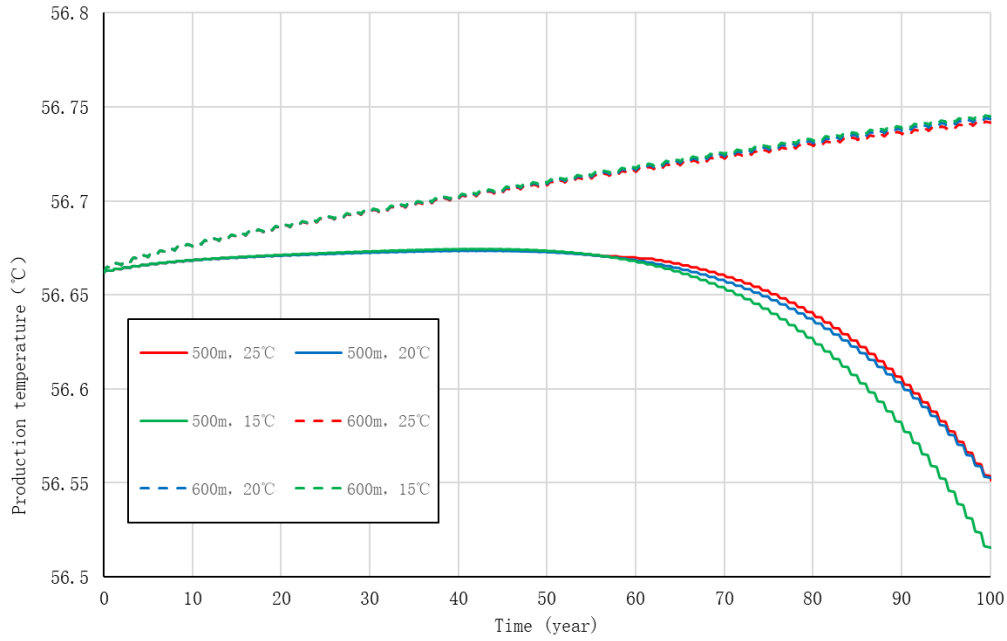


Figure 28: Comparison of the 500 m and 600 m well spacing temperature variation in 100 years.

4.4 Different production rate

Under 500 meters of well spacing, the temperature influence range of three reinjection temperatures under the reinjection rate of 70, 90, and 110 m³/h was compared. The simulation results are shown in Figure 29. The bottom hole temperature of the reinjection well was mainly controlled by the reinjection temperature, and the larger the rate is, the lower the bottom hole temperature will be. Different from them, the temperature influence range of the reinjection well ($\Delta t > 2^\circ\text{C}$) was more obviously affected by the reinjection rate and was less affected by the reinjection temperature. Larger reinjection rate and lower reinjection temperature results in a larger radius of the impact of temperature drop, but neither extended to the production Wells (in the case of 500m well spacing).

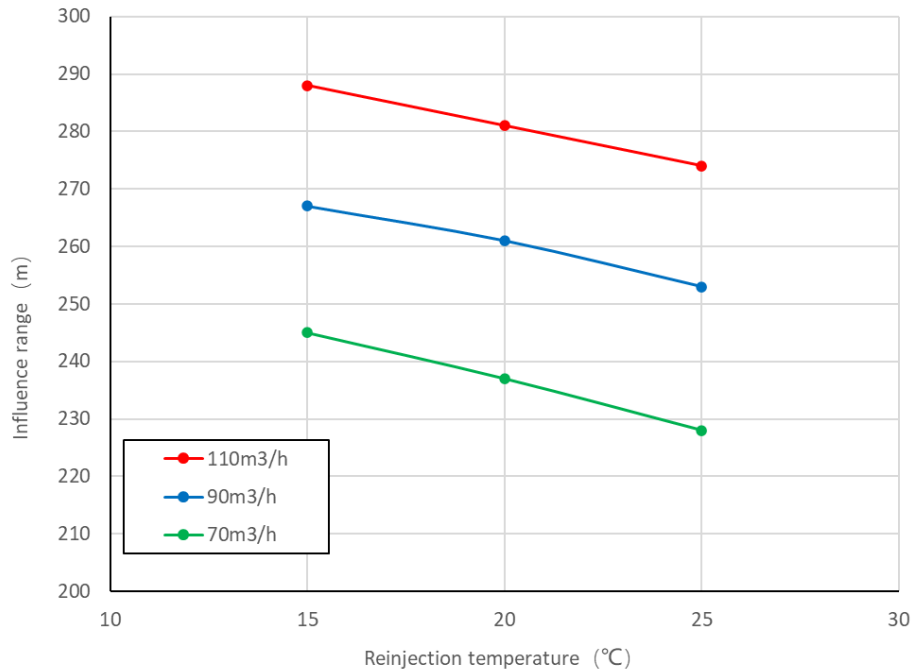


Figure 29: Comparison of temperature influence radius of reinjection after 100 years under different recharge amounts and different recharge temperatures (500m well spacing)

Different mining rates and reinjection temperatures for production wells will also lead to changes in production temperature. Figure 30 compares the influence of varying mining rates and reinjection temperatures on the production temperature with well spacing of 500m. It can be seen from the figure that: (1) the production temperature began to decline from 50 to 70 years, and the greater the reinjection rate, the earlier the temperature decrease occurs.; (2) the amount of reinjection has a more significant influence on the production temperature, while the impact of reinjection temperature on the production temperature was relatively limited.

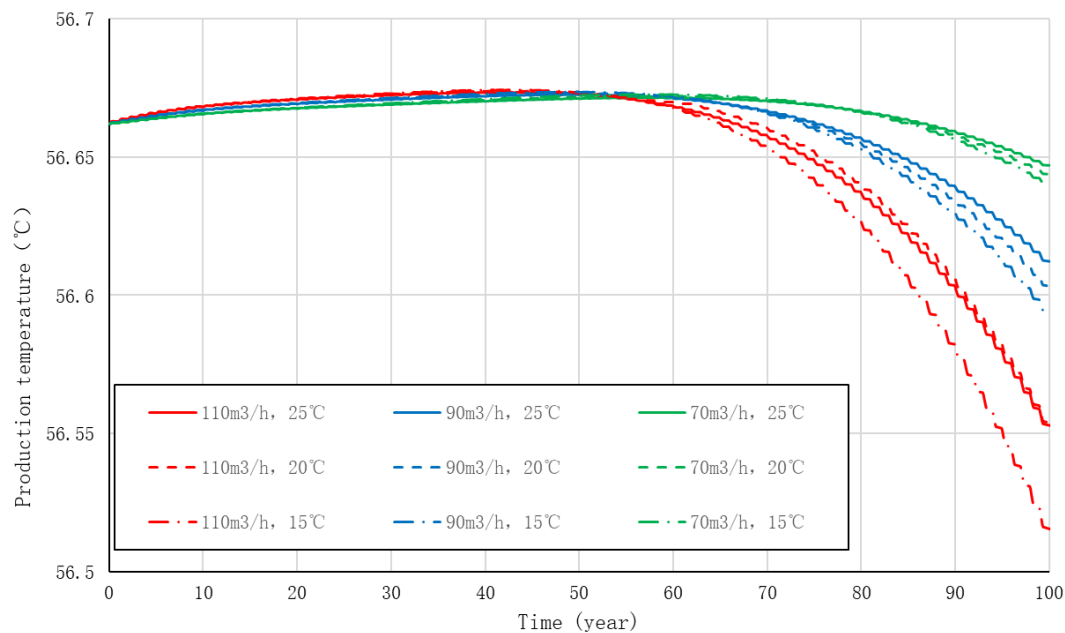


Figure 30: Comparison of temperature change of mining well under different reinjection rates and temperature (500m well spacing)

5. CONCLUSION

Based on the numerical model, reservoir response to different well spacing and different reinjection rate temperatures were compared, and the following conclusions were:

- 1) distributed and centralized mining schemes both have advantages and disadvantages. The distributed mode has less disturbance to the reservoir, while the centralized way is more conducive to maintaining the capacity.
- 2) Two well spacing schemes, 600 m and 500 m, were compared under the production rate of $110\text{m}^3/\text{h}$. No thermal breakthrough occurred even though the well spacing was 500 meters, but the temperature decreased after 100 years. Considering the heterogeneity of thermal storage and conductivity, it is recommended that the well spacing should be at least 500 meters under this production rate.
- 3) The larger reinjection rate and the lower reinjection temperature will increase the temperature influence radius and reduce the mining temperature, but the effect of the recharge rate is more prominent. In actual production, if the distance between the mining well and the recharge well is close, to prevent the thermal breakthrough occurrence, the first consideration should be to reduce the reinjection rate rather than increase the recharge temperature.

REFERENCES

- Wang J Y, Ma W B, Gong Y L, et al., Geothermal Utilization Technology, Chemical Industry Press: Beijing, 2005
- X. Li. Empirical analysis of the smog factors in Beijing-Tianjin-Hebei region Ecol. Econ., 32 (2016), pp. 144-150
- Air quality analysis of key regions and 74 cities in China Ministry of Ecology and Environment of the People's Republic of China (Original Ministry of Environment Protection of the People's Republic of China) (2015)
- J. Hou, M. Cao, P. Liu. Development and utilization of geothermal energy in China: current practices and future strategies Renew. Energy, 125 (2018), pp. 401-412
- Albert A., Asbjorn B., Bjorn H. B., et al., Environmental impact assessment of geothermal projects in Iceland. In: Proceedings world geothermal congress 2010, Bali, Indonesia, 25-29 April 2010.
- Soheil P., Rooholamin S., Saba O., Environmental monitoring of air, soil and surface water resources: A case study on meshkinshahr geothermal field development. In: Proceedings world geothermal congress 2010, Bali, Indonesia, 25-29 April 2010.
- Einar G., Helgi L., Ingólfur H., et al., Environmental issues related to the building of new power plants in the hengill area. In: Proceedings world geothermal congress 2010, Bali, Indonesia, 25-29 April 2010.
- Giovannoni A., Allegrini G., Cappetti G., 1981. First results of reinjection experiment at Larderello. Proceedings of 7th workshop on geothermal reservoir engineering, Stanford university, Stanford, CA, 77-83.
- Cappetti G., Giovannoni A., Ruffilli C., et al., 1982. Reinjection in the Larderello geothermal field. International Conference on Geothermal Energy, Florence, Italy, 11-14 May, pp. 395-407.
- Zarrouk S. J., O'Sullivan M. J., Croucher A. E., et al., 2006. Optimized numerical modeling of production from the poihipi dry steam zone: wairakei geothermal system. Proceedings of 31 Workshop on geothermal reservoir engineering Stanford University, Stanford, California, January 30-February 1, 2006 SGP-TR-179.

Yang et al.

Romagnoli P., Arias A., Barelli A., et al., An updated numerical model of the Larderello–Travale geothermal system, Italy. *Geothermics*, 2010, 39 (4): 292-313.